

Chapter 3

Testing of wavefront from lenses

3.1 Introduction

Wavefront-sensing techniques provide a perfect method for quantitative as well as qualitative understanding of the wavefronts emanating from optical systems. The measurement of the wavefront parameters will provide a means for proper selection of optical components depending upon the application needs.

Lens is one of the most important optical component used for wavefront manipulations. The measurements of lens parameters such as focal length, radius of curvature, and refractive index of the lens material as well as the shape of the wavefront provided by a lens are important for their proper selection in various applications. Many applications not only demand enhanced quality, but also require exact specification of lens-characteristics. In particular, an accurate knowledge of the refractive index of the glass materials can provide one with information about the materials' reflectance and transmittance. There are many methods for the determination of these lens parameters. These include liquid immersion methods and optical interferometric methods using shearing plates and gratings [3.1–3.17]. The interferometric methods compare the wavefront from the test lens with a reference plane wavefront for the determination of its flatness. Recently a method using Michelson interferometer was proposed [9]. This method has the advantage that the focus and radius of curvature of the lens were determined from positions of the lens, which resulted in a uniform field of view (single fringe corresponding to constant phase difference). But all the above-mentioned methods require a comparison with a physical plane wavefront, which may introduce some errors if this wavefront is not really uniform (plane) or does have some aberrations. In digital holography, the holograms recorded using a light-sensitive detector array could be reconstructed numerically, yielding both the amplitude and the phase of the signal wavefront [3.18,

3.19]. One of the greatest advantages of digital holographic interferometry is that one can compare the digitally reconstructed signal wavefront with any synthetically generated (computer-generated) wavefront during the reconstruction process. This means that the signal wavefront can be compared with an ideal wavefront rather than a physical one. This will improve the measurement accuracy of wavefront properties such as curvature and aberrations. This aspect of digital holography has already been used for a surface shape measurement [3.20]. Here digital holography is used as a single shot method for determination of various lens parameters as well as to investigate wavefronts produced by lenses [3.14, 3.15]. The signal wavefront from the test lens is compared with a synthetically generated reference plane wavefront for parallelism to determine the focal length and radius of the curvature of lenses. These parameters are then used in the thin lens formula for the determination of the refractive index of the lens material. The wavefront curvature as well as amount of deviation of test lens from collimation position is also determined by comparing the shape of the wavefront produced by the lens with an ideal plane computer generated wavefront. Here the method is presented for testing of thin bi-convex lenses. But the method could be extended to test any simple lens or a lens system.

3.1. Measurement of parallelism of the wavefront

The experimental geometry for the determination of the focal length of lenses is shown in Fig. 3.1. Light from a laser source is expanded using a spatial filtering assembly, which could be an optical fiber. This expanded beam is passed through the collimating lens. The collimating lens is so adjust that reconstructed the phase at the detector plane corresponds to a plane wave. The collimated beam is split into two using a beamsplitter. One of the two beams is then focused and passed through a pin-hole. The test lens is kept at a position nearly equal to its focal length from the pin-hole. The test lens is mounted on a translation table so that it can be moved along its optic axis. The wavefront from the test lens interferes with a slightly off-axis plane reference wavefront at the detector or hologram plane employing Mach-Zehender geometry. The microinterferogram (hologram) is recorded by a CCD camera and stored in a PC. The coordinate system for the recording process is shown in Fig. 3.2.

The complex amplitude of the interference pattern at the hologram plane according to Fresnel-Kirchoff diffraction integral is given by

$$U_H(\xi, \eta) = \frac{i}{\lambda d} \exp\left(-i\frac{2\pi}{\lambda}d\right) \iint_{-\infty}^{\infty} U_L(x, y) \times \exp\left\{-i\frac{\pi}{\lambda d}\left[(\xi-x)^2 + (\eta-y)^2\right]\right\} dx dy + A \exp\left(-i\frac{2\pi}{\lambda}\xi \sin\theta\right) \quad (58)$$

where $U_L(x, y)$ is the complex amplitude of the wavefront at a tangential plane just after the back surface of the lens, d is the distance between the lens and the hologram plane, and λ is the wavelength of the light used. The second term on the right-hand side is complex amplitude of a plane wavefront of amplitude A incident an angle θ with the x axis. The interferogram is recorded as an intensity pattern with its intensity as the square of the absolute of complex amplitude in Eq. (58).

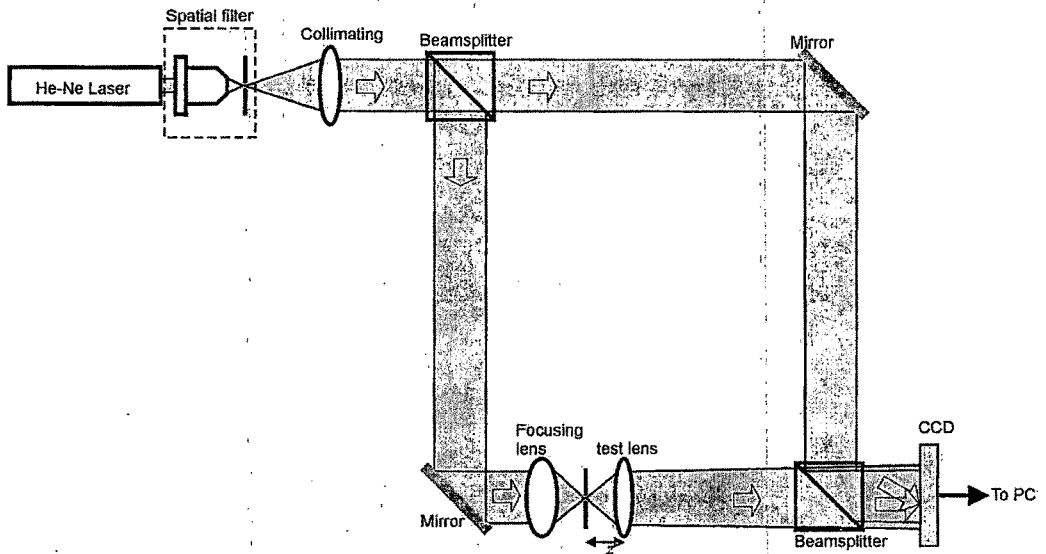


Fig. 3.1: Experimental setup for exact measurement of focal length of lens using digital holography. Test lens was mounted on a translation stage.

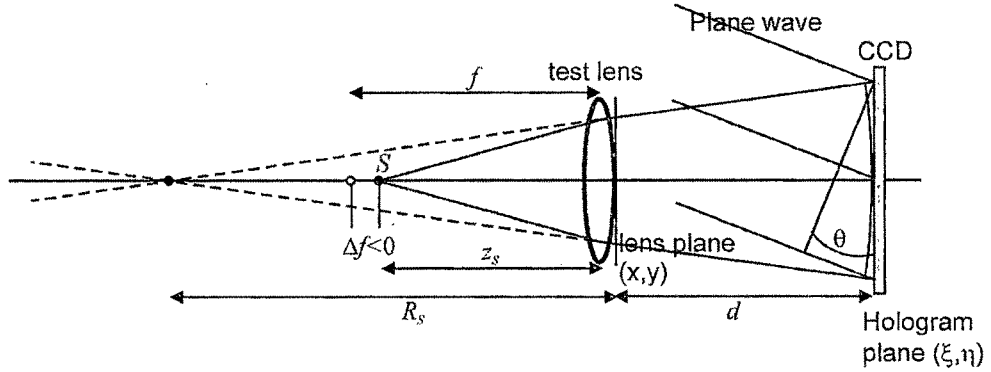


Fig. 3.2: Coordinate system of the recording as well as reconstruction geometry. The wavefront due to a lens placed just inside the focus is also shown. The y and η axes are into the plane of the paper.

During the reconstruction process, the hologram is illuminated with a conjugate of the reference wavefront, and the complex amplitude $U_L(x, y)$ of the original signal wavefront from the test lens can be computed numerically either by using the Fresnel transform or Angular Spectrum Propagation approach. As mentioned earlier the main advantage of the digital holographic process is the direct computation of phase from the computed complex amplitude. The phase of the wavefront at a plane tangent to the back surface of the test lens is

$$\phi_w = \arctan \frac{\text{Im}[U_L(x, y)]}{\text{Re}[U_L(x, y)]} \quad (59)$$

This phase depends upon the radius of curvature of the wavefront after the test lens. This radius of curvature of the wavefront R_w depends upon the amount of deviation from collimation position (Δf) and focal length of the lens f and is given by [3.7]

$$R_w = \frac{f^2}{\Delta f} \quad (60)$$

The phase at the plane tangent to the back surface of the test lens can also be written as (see Fig. 3.2 for details)

$$\phi_w = \frac{2\pi}{\lambda} \sqrt{x^2 + y^2 + R_w^2} \quad (61)$$

It can be seen that the phase depends upon the Δf and hence the radius of curvature of the wavefront passing through the test lens, and when the beam is exactly collimated this phase is constant across the plane. Digital holograms of the wavefront from the test lens at various positions of the lens from the point source are recorded. Fig. 3.3 shows one of the simulated holograms using a test lens with a focal length of 50 mm and $\Delta f = 0.1$ mm. The hologram was simulated considering a CCD array of 1024×1024 pixels of $9.8 \mu\text{m}$ size and an 8 bit dynamic range; the reference wave was introduced at an angle of 1° with respect to the ξ axis (see Fig. 3.2) taking into consideration the spatial frequency limitation. The distance from the test lens to the hologram plane was 0.5 m. Only a portion of the hologram of 512×512 pixels is shown. The phase of the signal wavefront from the lens is computed using the Angular spectrum propagation integral.

The computed phase of the wavefront from the test lens is then compared with the phase of a synthetic plane wavefront used as a reference. The reference phase $\phi_R(x, y)$ introduced digitally. The interference phase between the computed phase of the signal from the test lens $\phi_w(x, y)$ and the digitally input plane wavefront $\phi_R(x, y)$ is directly obtained by subtraction.

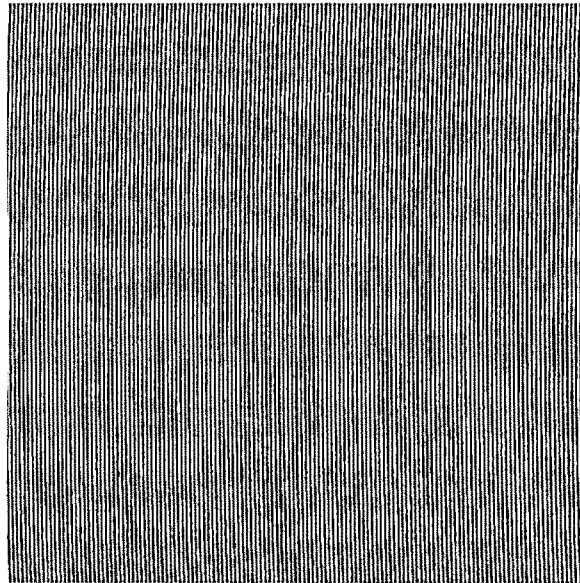


Fig. 3.3: Simulated hologram for a test lens of 50 mm focal length and $\Delta f = 0.1$ mm.

It can be seen that the phase map will contain concentric circles, with each 2π phase change representing a depth change of λ , when the beam is not perfectly collimated. When the beam is perfectly collimated the phase map will yield a single fringe corresponding to the constant phase difference between the two wavefronts. Therefore by moving the lens along the optic axis and comparing the computed phase with the phase of a plane wavefront, the position where a single fringe results can be found. This is the collimation position, and this position gives the focal length of the lens. Fig. 3.4 shows the change in the radius of curvature of the wavefront with when test lens is moved from inside focus to focus to outside focus. Fig. 3.5 shows the phase maps computed from the simulated holograms and the digitally introduced plane wavefront for a test lens with a focal length of 50 mm as it is shifted from its collimation position by different amounts. It can be seen that as the lens is moved from inside focus the fringes in the phase map decrease, become single fringe at focus, and start to appear again as the lens is moved outside focus.

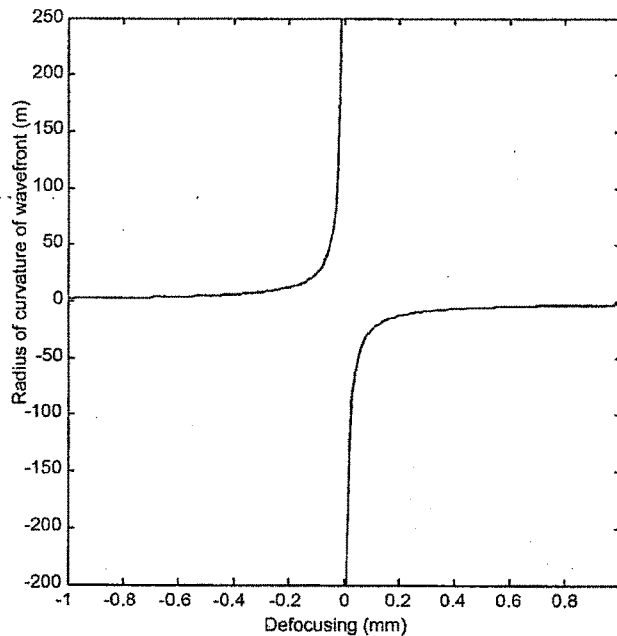


Fig. 3.4: Change of the radius of curvature of the wavefront with defocusing of the test lens.

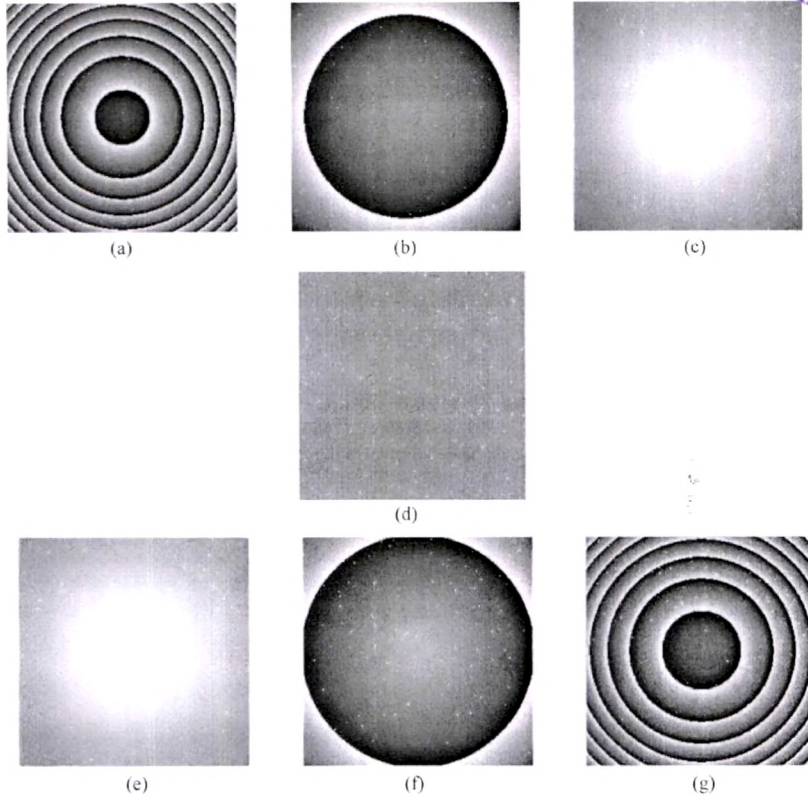


Fig. 3.5: Simulated phase maps for different defocusing for a test lens with a focal length of 50 mm. (a) 0.5 mm inside focus, (b) 0.1 mm inside focus, (c) 0.02 mm inside focus, (d) at focus, (e) 0.02 mm outside focus, (f) 0.1 mm outside focus, and (g) 0.5 mm outside focus.

Experiments were conducted with a test lens of effective focal length 50.2mm having a clear aperture of 25.4mm. The lens was mounted on a manual translation stage with 10 μ m resolution. Holograms were recorded for various positions of the lens as it was moved from inside focus to focus to outside focus. A CCD chip having 580 \times 760 pixels with 9.8 μ m pixel pitch and 8-bit dynamic range was kept 15cm from the test lens as the recording device. Fig. 3.6 shows the recorded hologram for a defocusing of $\Delta f=6$ mm ($\Delta f=f-z_s$, where z_s is the distance of the lens from the point source). The laser source used had a vacuum wavelength of 633nm.

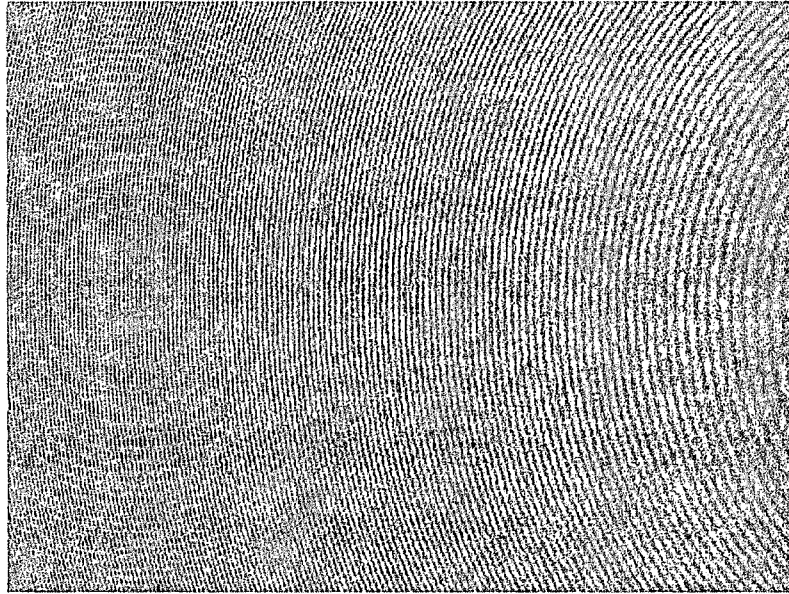


Fig. 3.6: Experimentally recorded hologram for a test lens of focal length 50.2mm and clear aperture of 25.4mm and $\Delta f=6\text{mm}$.

The reconstructed phase maps were used to determine the parallelism of the wavefronts from the lens. Fig. 3.7 shows the reconstructed phase maps for different lens positions. It can be seen that as distance between the lens and the point source nears f , the number of phase fringes decrease, indicating better parallelism. The wavefront is perfectly collimated when this distance is exactly f as indicated by fringe free phase map shown in Fig. 3.7c.

The sensitivity of the focal length measurement depends upon the least detectable Δf , which in turn depends upon the minimum detectable phase difference. Considering that a minimum phase variation of π radians across the phase map is necessary to detect the deviation of lens from collimation position, the sensitivity of the system can be decided. The change in sensitivity of the system for testing of wavefront parallelism with the change in focal length of the test lens is plotted in Fig. 3.8.

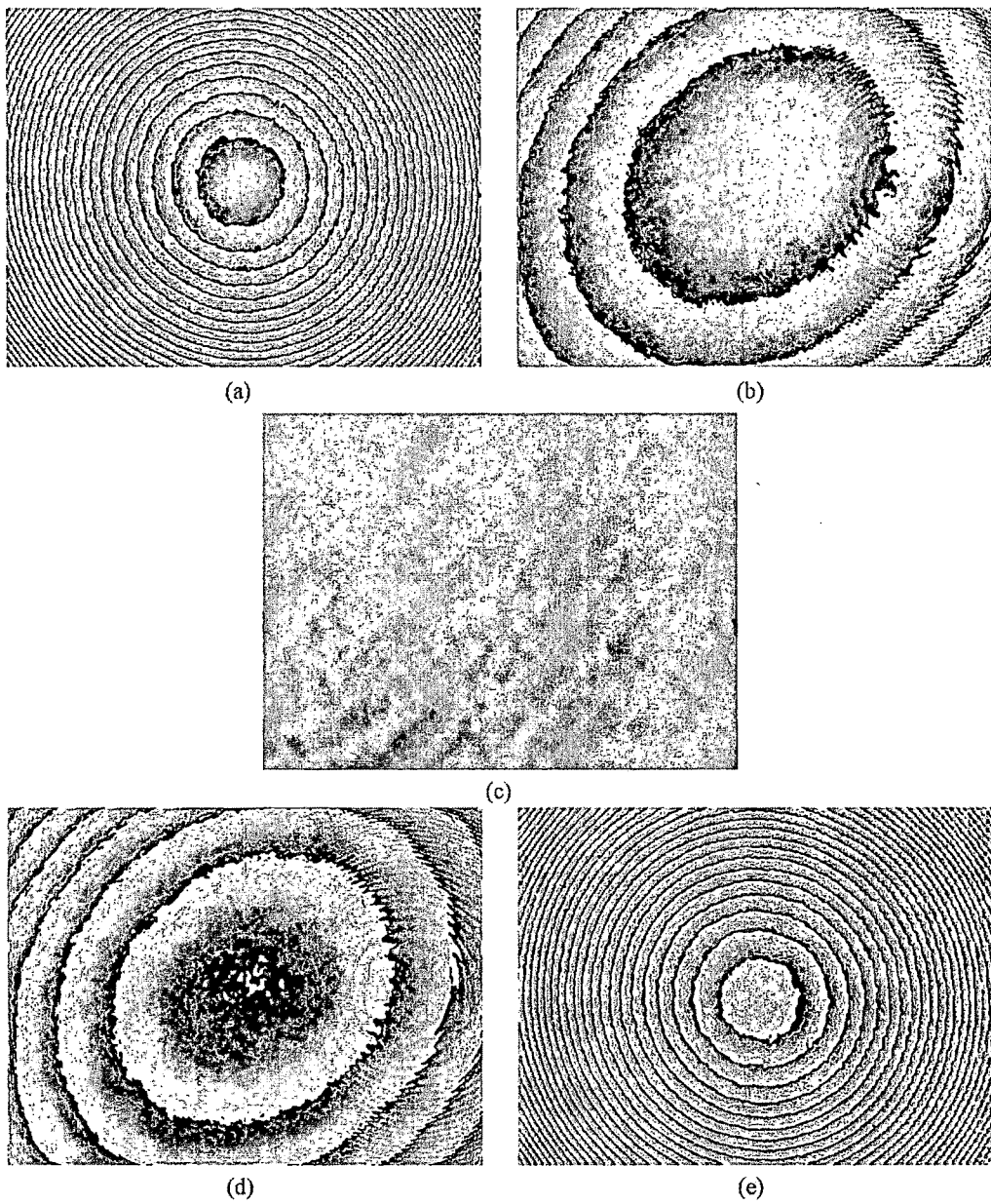


Fig. 3.7: Experimentally observed phase maps for different Δf for a test lens with a focal length of 50.2 mm. (a) 4.5 mm inside focus, (b) 0.65 mm inside focus, (c) at focus, (d) 0.8 mm outside focus, (e) 4.3 mm outside focus.

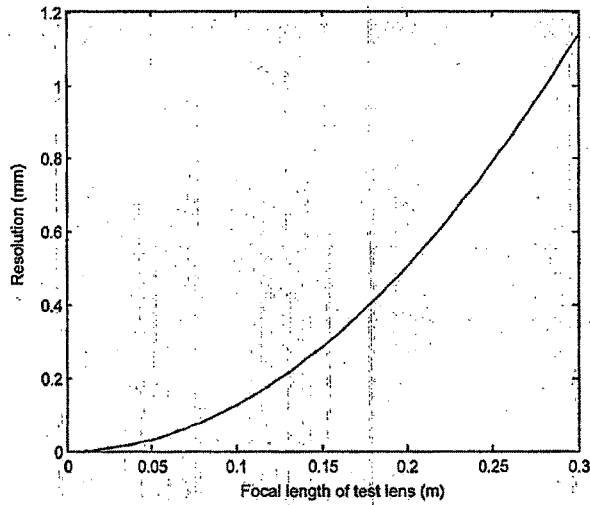


Fig. 3.8: Change in sensitivity in the measurement of wavefront parallelism.

3.2 Measurement of wavefront radius of curvature

The radius of curvature (R_w) the emerging wavefront from the lens is measured directly from the reconstructed phase. The continuous phase distribution at a tangential plane after the lens ϕ_w is obtained after unwrapping. The line along the center y -direction passes through the point of maximum phase change (Fig. 3.9). It can be seen from Fig. 3.9 that the radius of curvature of the wavefront can be directly obtained by determining the change in phase of the wavefront from the maximum phase.

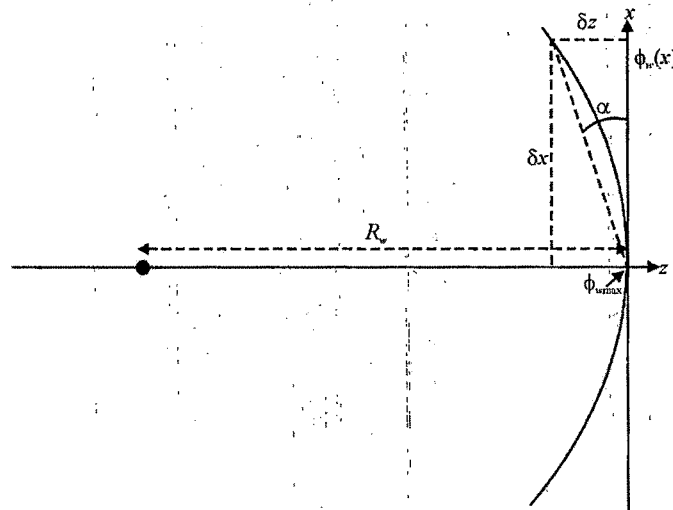


Fig. 3.9: Phase change at the tangential plane after the lens. From the change in phase the change in height of the wavefront can be calculated.

From Fig.3. 9, the change in height of the wavefront with position depends on the obtained phase through

$$\delta z = \frac{\phi_{wmax} - \phi_w(x)}{2\pi} \lambda \quad (62)$$

The radius of curvature of the wavefront can then be written in terms of the change in height and x-position as

$$R_w = \frac{\sqrt{\delta x^2 + \delta y^2}}{2 \sin \alpha} \quad (63)$$

When angular spectrum propagation is used for reconstructions the pixel size at the reconstructed plane is same as the sensor pixel size. So δx is just the product of the number of pixels N and pixel size in x-direction Δ ($\delta x = N \times \Delta$).

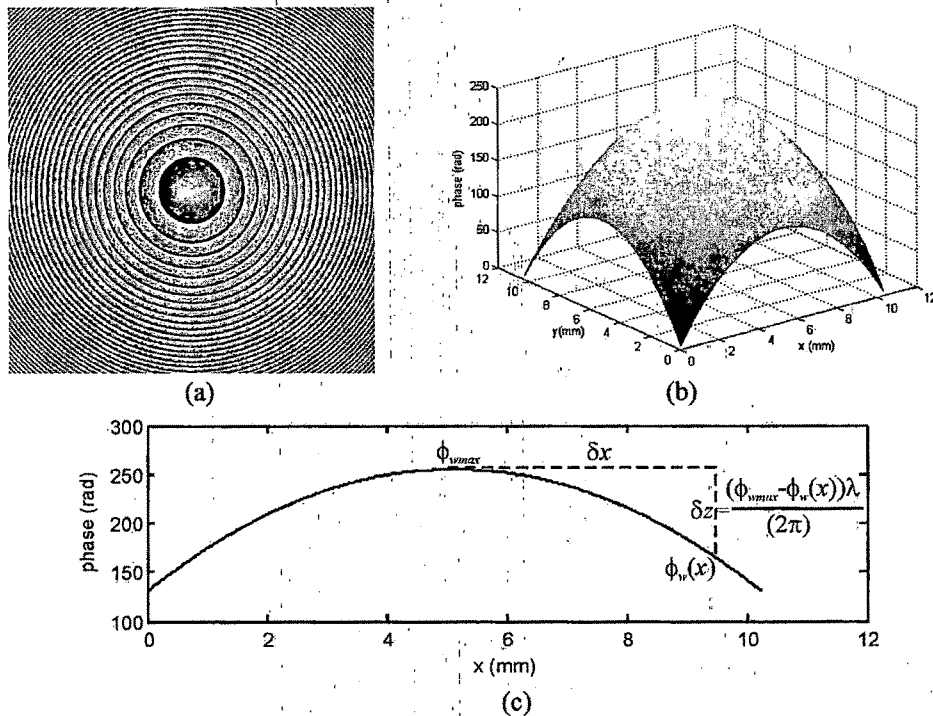


Fig. 3.10: (a) Simulated phase map for the wavefront exiting from a 50m focal length bi-vonvex lens and $\Delta f = 2.5\text{mm}$ there by providing an expanding wavefront (b) Continuous phase distribution after unwrapping Fig. 10a, (c) Phase change along the central x-direction.

Fig. 3.10 shows the simulated phase map for a 50mm focal length lens for $\Delta f=2.5\text{mm}$ and the obtained continuous phase distribution after unwrapping. The line profile of the phase change along the central x -direction is shown in Fig. 3.10c.

Calculated radius of curvature R_w from the line plot for the expanding wavefront in Fig. 3.10 was 999.997mm, which matches with the value obtained using Eq. (61). Experimentally obtained phase profile for a test lens of focal length 50.2mm with $\Delta f=6.05\text{mm}$ is shown in Fig. 3.11a. The three dimensional profile of the wavefront after unwrapping is shown in Fig. 3.11b. The profile of the wavefront along the central x -direction (along the solid line shown in Fig. 3.11b) is plotted in Fig. 3.11c.

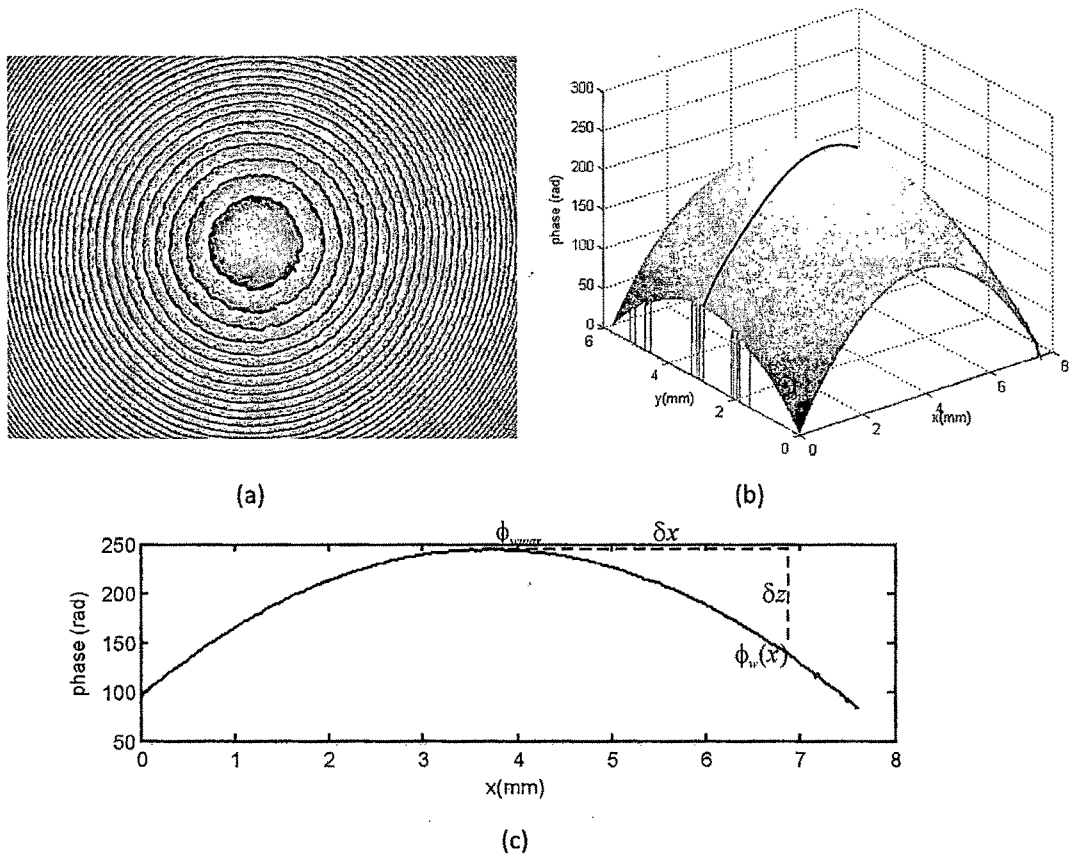


Fig. 3.11: (a) Experimentally obtained phase map for a test lens of focal length 50.2mm and $\Delta f=6.05\text{mm}$. (b) The continuous phase distribution corresponding to Fig. 11a obtained after unwrapping. (c) Profile of the wavefront along the central x -direction (solid line in Fig. 11b). The calculated radius of curvature of the wavefront from this line profile was 417.89mm, which is close to the expected value of 416.53mm.

Curvature of the wavefront was computed using Eq. (63). The computed value was 417.89mm which is very close to expected value of 416.53mm calculated using Eq. (61). Several points on the wavefront profile were used for R_w calculation and the average of these will give the best approximation. The method was tested for several Δf (for converging as well as diverging wavefronts) and the average error in finding the radius of curvature of the wavefront was estimated to be less than 0.8%.

3.3 Measurement of focal length of test lens

Focal length of the test lens can be measured from the distance at which exact collimation results, which is basically the distance of the point source from test lens when the phase map does not contain any fringes. A better estimation of the focal length of the test lens could be obtained from the change in radius of curvature of the exiting wavefront for different deviations from the collimation position (Δf). The equations for the radius of curvature of the wavefront exiting from the test lens of focal length f placed Δf_1 and Δf_2 away from the collimation position are given by,

$$R_{w1} = \frac{f^2}{\Delta f_1} \quad (64)$$

$$R_{w2} = \frac{f^2}{\Delta f_2} \quad (65)$$

Subtracting Eq. (64) from Eq. (65) and re-arranging the terms

$$\Delta f_2 - \Delta f_1 = \delta = f^2 \left(\frac{R_{w1} - R_{w2}}{R_{w1} R_{w2}} \right) \quad (66)$$

$$f = \sqrt{\left(\frac{R_{w1} R_{w2}}{R_{w1} - R_{w2}} \right) \delta} \quad (67)$$

where δ is the difference between the de-collimation positions, which is readily available from the translation stage reading. From the phase maps at two de-collimation positions (Δf_1 and Δf_2) the radius of curvatures R_{w1} and R_{w2} can be determined and by using this in Eq. (67), focal length of the lens is obtained.

Fig. 3.12 shows the simulation results for measurement of lens focal length. The test lens had a focal length of 50mm. The test lens was kept at two de-collimation

positions $Df_1=5\text{mm}$ and $Df_2=2.5\text{mm}$. The obtained phase maps are shown in Fig. 3.12a and 3.12b respectively. Fig. 3.12c represents the variation in phase along the central x-direction for the two cases. The calculated radius of curvatures using the phase data were 500.001mm and 999.997m respectively compared to theoretical results calculated using Eq. (61) of 500mm and 1000mm respectively. The focal length calculated using these two radiuses of curvature values comes out to be 50.002mm. The average error in focal length determination from simulations was less than 0.005%.

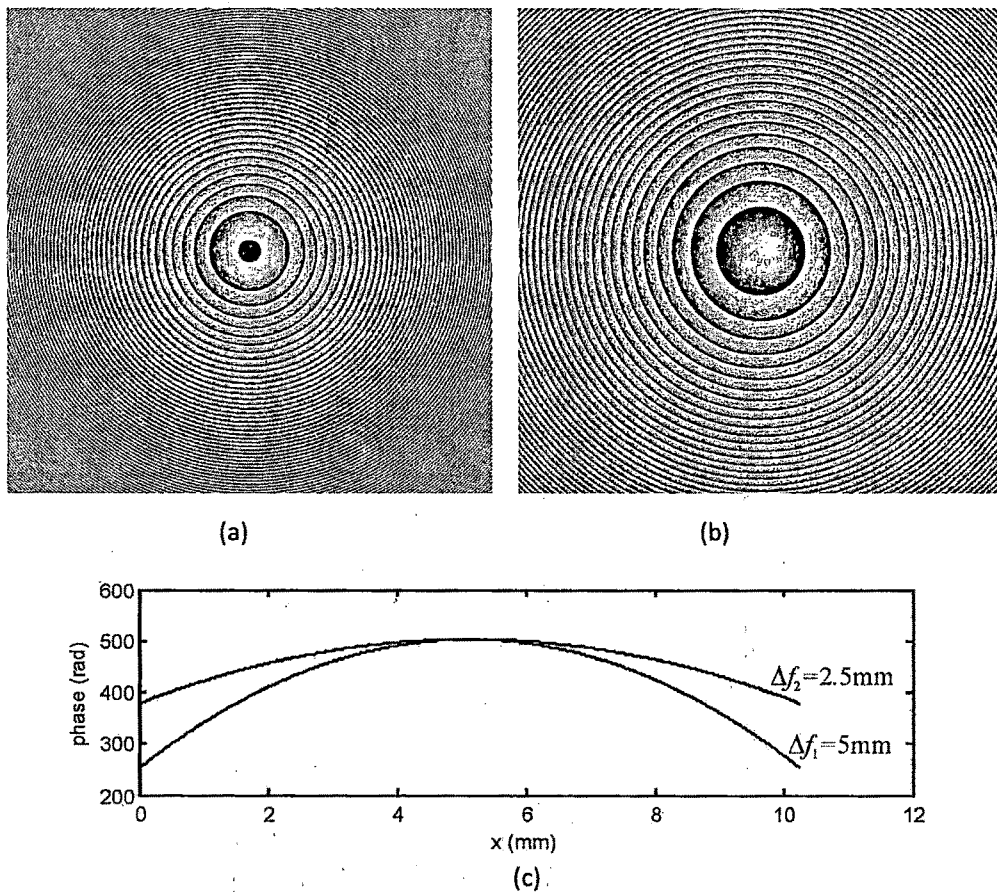


Fig. 3.12: Simulation results for measurement of wavefront curvature to determine focal length of test lens (a) Reconstructed phase of the wavefront when test lens is de-collimated by 5mm, (b) Phase profile when the de-collimation was 2.5mm, (c) Profile of phase along the center x-direction for both de-collimations. The change in curvature is clearly visible.

Experiments were carried out on a 50.2mm focal length test lens de-collimated by various distances. Fig. 3.13a and 3.13b shows the experimental results for two de-collimation positions $\Delta f_1=6.05\text{mm}$ and $\Delta f_2=3.83\text{mm}$ respectively. The profile of the phase along the center x-direction for both these de-collimations is shown in Fig. 3.13c. The computed curvature of the wavefront for these two de-collimation position were 417.89mm and 660.24mm respectively compared to theoretical values of 0.416m and 0.658m respectively, computed using Eq. (61). The calculated focal length using these values of de-collimation and radiuses of curvature was 50.24mm, which is quite comparable with the value specified by the manufacturer, taking into account the source wavelength.

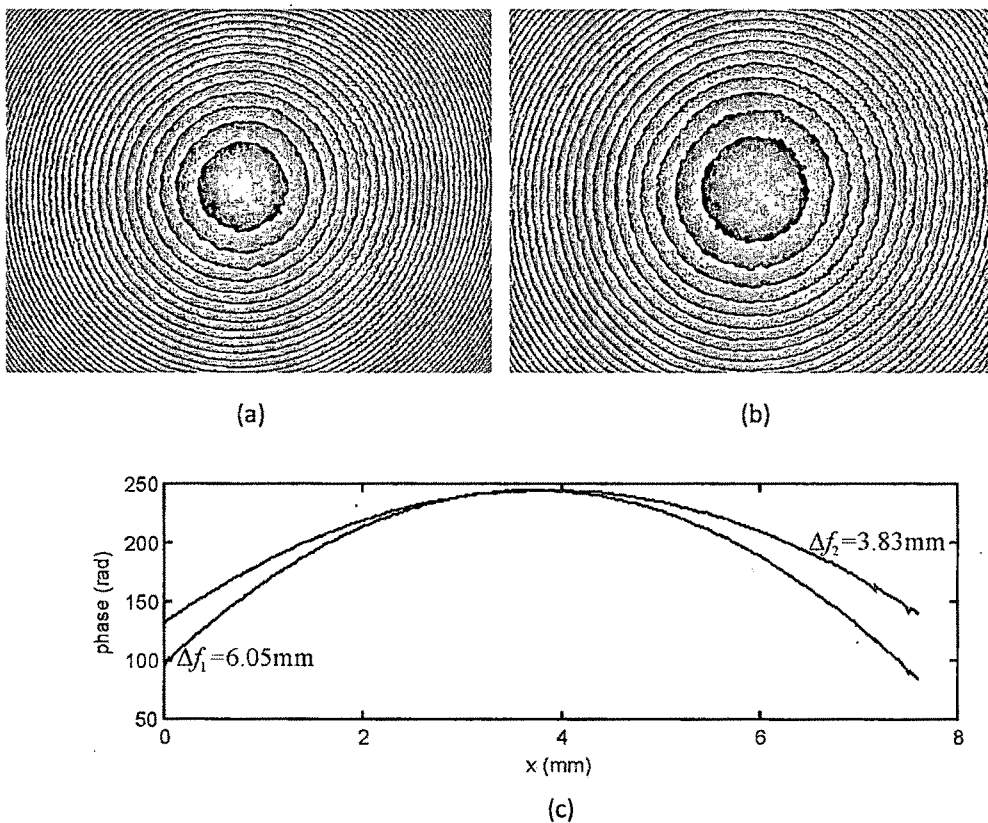


Fig. 3.13: Experimental results for focal length measurement of test lens with $f=50.2\text{mm}$. (a) Reconstructed phase of the wavefront when test lens is de-collimated by 6.05mm, (b) Phase profile when the de-collimation was 3.83mm, (c) Profile of phase along the center x-direction for both de-collimations. Computed focal length using this data was 50.27mm

Table 3.1 gives the computed radius of curvature for different de-collimation of the test lens. The measured R_w for various de-collimations were used for finding the focal length of test lenses. This is tabulated in Table 3.2. Average value of focal length from various de-collimation distances was found to be 50.27 ± 0.21 mm. The error in determination of focal length depends upon the error in determination of radius of average in determination of focal length was less than 0.8%.

Table 3.1: Radius of curvature of wavefront

Sr. No.	Δf (mm)	Theoretical R_w (mm)	Experimental R_w (mm)
1	6.05	416.53	417.89
2	4.47	563.77	565.39
3	4.02	626.88	629.47
4	3.83	657.97	660.24

Table 3.2: Focal length of test lens (manufacturer specified $f=50.2$ mm)

Sr. No.	Δf (mm)		R_w (mm)		Focal length (mm)
1	Δf_1	6.05	R_{w1}	417.89	50.31
	Δf_2	4.47	R_{w2}	565.39	
2	Δf_1	6.05	R_{w1}	417.89	50.23
	Δf_2	4.02	R_{w2}	629.47	
3	Δf_1	6.05	R_{w1}	417.89	50.27
	Δf_2	3.83	R_{w2}	660.24	
4	Δf_1	4.47	R_{w1}	565.39	49.99
	Δf_2	4.02	R_{w2}	629.47	
5	Δf_1	4.47	R_{w1}	565.39	50.19
	Δf_2	3.83	R_{w2}	660.24	
6	Δf_1	4.02	R_{w1}	629.47	50.65
	Δf_2	3.83	R_{w2}	660.24	
Average focal length					50.27 ± 0.21 mm

3.4 Measurement of lens radius of curvature

The radius of curvature is also determined using a similar technique but with a different experimental setup. The experimental setup is shown in Fig. 3.14. A collimated beam is focused by a large focal length lens L_A on to the front surface of the test lens. Lens L_A acts as an autocollimator. The wavefront reflected from the front surface of the test lens will be collimated by this autocollimator only at two positions of the test lens. One is when the beam from L_A focuses on the center of curvature of the test lens and the other when it focuses on its front surface (both these positions are shown in Fig. 3.14). At these two positions since the wavefront emanating from L_A is collimated the phase map will contain only a single fringe. The radius of curvature of the test lens is therefore determined by moving the test lens along its optic axis. The reflected light from the lens surface interferes with an off-axis plane wavefront to form the hologram. The radius of curvature of the front surface of the test lens R_l is determined from the positions where a single fringe phase map results using the formula (see Fig. 3.14 for details)

$$R_l = z_2 - z_1 \quad (68)$$

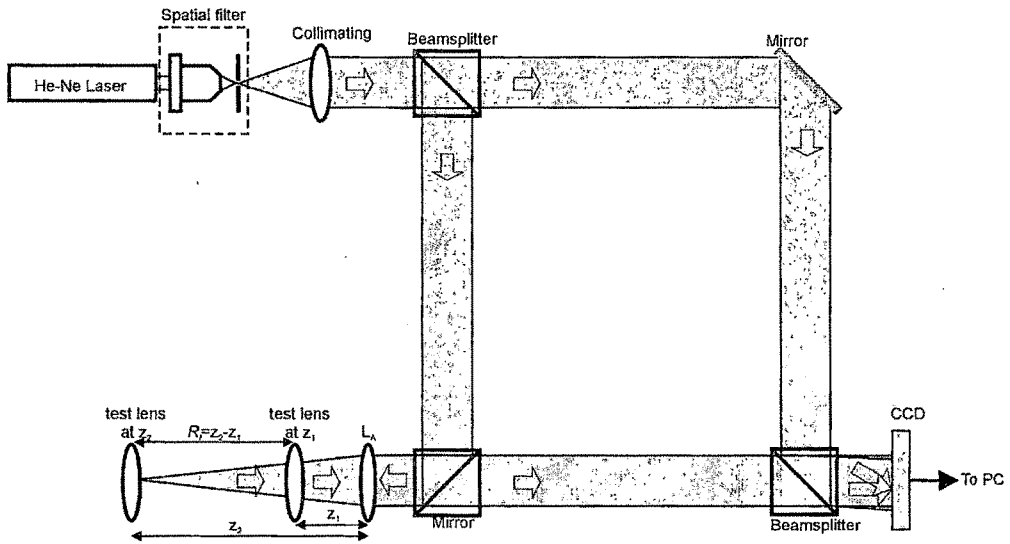


Fig. 14: Experimental setup for lens radius of curvature measurement using digital holography. The auto-collimating lens has a larger focal length than the test lens.

It is obvious that the focal length of the auto-collimating lens should be longer than that of the test lens. Fig. 3.15 shows the simulation results for a bi-convex test lens of focal length 50mm made up of BK7 glass. The radius of curvature calculated using thin lens equation is 51.5mm. The auto-collimating lens considered had a focal length of 100mm. It can be seen that the at two points the wavefront from the auto-collimating lens become parallel, one when it focuses the beam to the center of curvature of the front surface of the test lens and second when it focuses the light on to the front surface of the test lens.

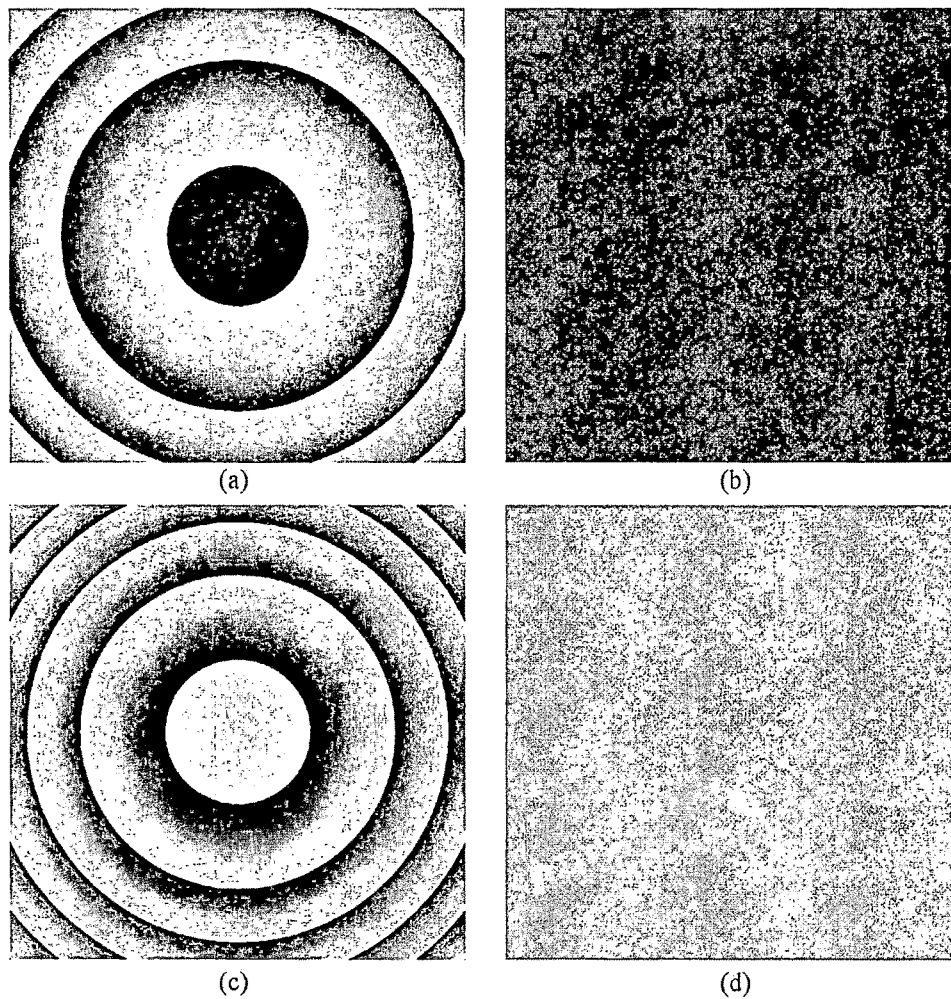


Fig. 3.15: Obtained phase maps from simulations for various positions of the test lens (focal length of 50 mm) from the auto-collimating lens. (a) 47 mm, (b) $z_1 = 48.5$ mm, (c) 52mm, (d) $z_2 = 100$ mm. Radius of curvature of the test lens is obtained from the difference in the two positions providing a fringe free phase map and is $R_f = z_2 - z_1 = 51.5$ mm.

Experiments were carried out on a 50.2mm focal length bi-convex lens using an auto-collimating lens of focal length 100mm. Reconstructed phase profiles for different positions of the test lens is shown in Fig. 3.16. Single fringe phase maps were observed at position $z_1=48.22\text{mm}$ and $z_2=99.96\text{mm}$. The computed radius of curvature of the front surface of the test lens is then 51.74mm, which is 0.5% outside the theoretically calculated value of 51.5mm. The radius of curvature of the back surface was also determined using the same procedure.

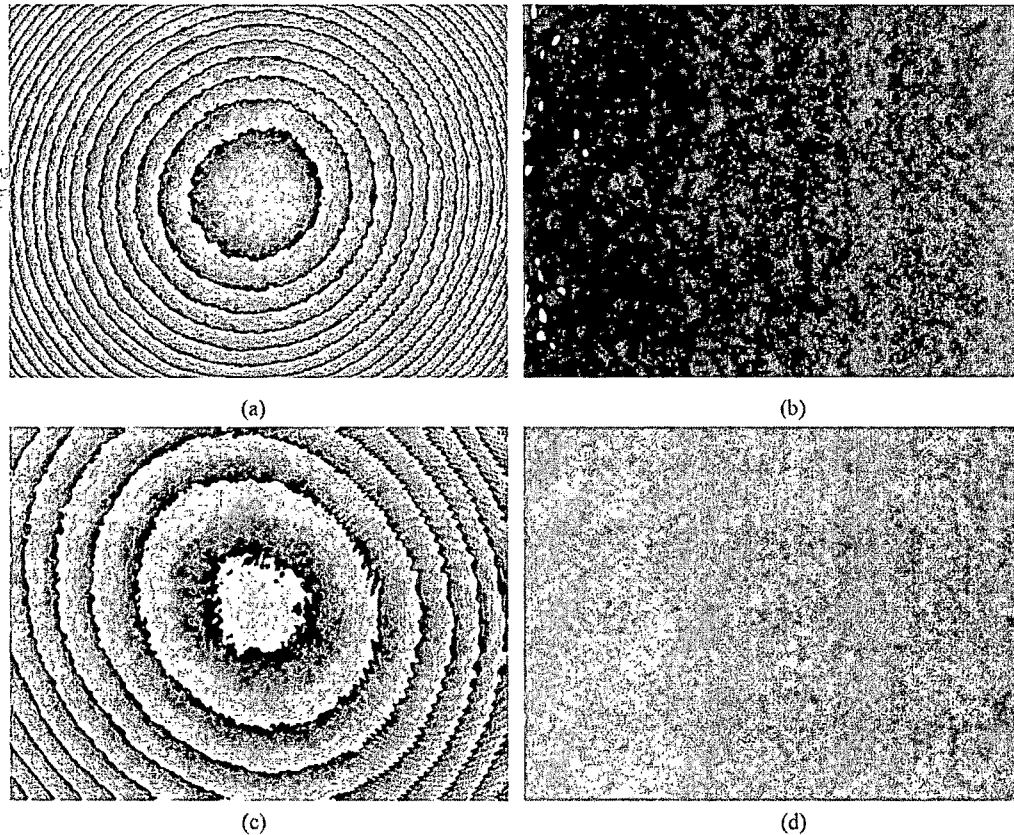


Fig. 3.16: Experimentally obtained phase maps for various positions of the test lens (focal length of 50.2 mm) from the auto-collimating lens of focal length 100mm. (a) 45 mm, (b) $z_1=48.22$ mm, (c) 55mm, (d) $z_2=99.96$ mm. Radius of curvature of the front surface of the test lens is obtained from the difference in the two positions providing a fringe free phase map and is $R_f=z_2-z_1=51.74\text{mm}$.

3.5 Determination of the Refractive Index

The refractive index is determined by using the lens equation with thin lens approximation. It is given by,

$$n = 1 + \frac{1}{f} \left(\frac{R_1 R_2}{R_2 - R_1} \right) \quad (69)$$

where R_1 and R_2 are the radii of curvature of the two surfaces of the test lens, and f is the measured focal length. R_2 is negative by sign convention for a biconvex lens. The error in measurement of refractive index depends upon the error in measurement of the focal length as well as the radius of curvature of the lens surfaces. The error in the measurement is found by differentiating Eq. (69) partially with respect to R_1 and f . Therefore the error in measurement can be written as

$$dn = \pm \left[\frac{1}{f} \left\{ dR_1 \left(\frac{R_2}{R_2 - R_1} \right) + dR_2 \left(\frac{R_1}{R_2 - R_1} \right) \right\} - \frac{(n-1)df}{f} \right] \quad (70)$$

where dn is the error in measurement of the refractive index, n is the measured refractive index, dR s are the errors in the measurement of the radii of curvature of the two surfaces of the test lens, and df is the error in measurement of the focal length. The error in the measurement of the refractive index depends upon the error in the focal length measurement and the radius of curvature measurement, and the error in the measurement of the radius of curvature depends only on the focal length of the auto-collimating lens. For a biconvex lens $R_2 = -R_1$, and Fig. 3.17 plots the change in the error of measurement in the refractive index as a function of focal length of the test lens (biconvex) for various focal lengths of the auto-collimating lens (lenses made up of BK7 glass with a refractive index of 1.51509 at 633 nm were considered [3.21]).

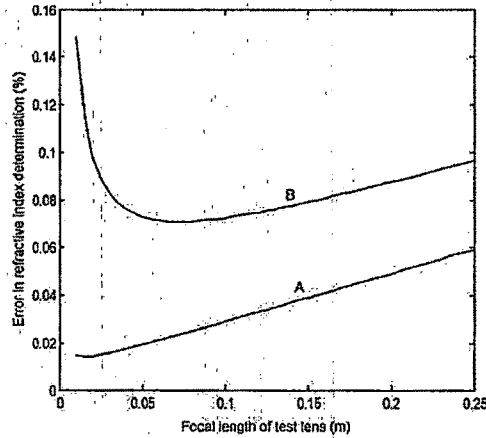


Fig. 3.17: Error in the determination of the refractive index. The differences of focal lengths between the test lens and the auto-collimating lens were (A) 10 mm and (B) 50 mm.

It can be seen that when an auto-collimating lens of focal length just greater than the focal length of the test lens is used, the error is the least (curve A). This is because the minimum detectable defocusing increases with the focal length of the auto-collimating lens. Therefore the error in measurement of the radius of curvature of the test lens will be the smallest when an auto-collimating lens, with a focal length just longer than the test lens, is used. As the focal length difference between the test lens and the auto-collimating lens increases, the error increases (as indicated by curve B). Therefore by choosing an auto-collimating lens of proper focal length the measurements could be made more accurate.

With the measured focal length and radius of curvature values using auto-collimating lenses of various focal lengths, the refractive index of the lens material was found to be 1.51471 ± 0.00012 which comes very close to the literature value of 1.51509 at 632.8nm for BK7 glass material [3.21].

3.6 Discussions and Conclusion

Some of the possibilities offered by the digital holography in the field of optical testing were illustrated by using it for complete characterization of simple lenses and wavefront produced by them. The digital reconstruction process involved in digital holography makes it a versatile tool to obtain rapidly from a single hologram a wide range of information on the wavefronts produced by lenses, which can be used to determine their different parameters like focal length, lens radius of curvature as well as the refractive index of the lens material.

The method can be used to test the parallelism of the wavefronts. Since the method can be used to determine the amount and sign of the curvature of the wavefront, it could be used for the exact determination of the collimation position for a lens. Focal length of the lens is obtained from measuring the change in curvature of the wavefront from lens. This is achieved directly from the computed phase of the wavefront from numerical reconstruction of holograms. Since the three dimensional profile of the wavefront so becomes available, focal length measurement becomes very simple, by comparing the wavefront curvatures for different de-collimation positions. The determination of the radius of the curvature involves a slightly more complex process of using an auto-collimating lens to determine the two positions where a perfectly

collimated wavefront results. The distance between these two positions directly yields the radius of curvature of the lens surface.

The technique can also be used to determine the refractive index of simple thin lenses accurately from the measured focal length and radius of curvature values. Here simulations and experiments were done for the case of biconvex lenses. But the method can be used for the parameter measurement of other types of lenses as well. For example, in the case of a concave lens, the focal length could be determined using the experimental setup shown in Fig. 1.1, using the concave lens in combination with a convex lens and finding the effective focal length. The focal length of the concave lens can be determined from the prior knowledge of the focal length of the convex lens. The procedure for the determination of the radius of curvature is the same as that for the convex lens. The method could also be extended to test the curvature and deviations from the plane nature of mirrors as well as other optical elements.

References

- [3.1] G. Smith, "Liquid immersion method for the measurement of the refractive index of a lens," *Appl. Opt.* **21**, 755 (1982).
- [3.2] R. S. Kasana and K. J. Rosenbrunch, "The use of plane parallel plate for determining the lens' parameters," *Opt. Commun.* **46**, 69 (1983).
- [3.3] R. S. Kasana, S. Boseck, and K. J. Oesenbrunch, "Use of a grating in a coherent optical processing configuration for evaluating the refractive index of a lens," *Appl. Opt.* **23**, 757 (1984).
- [3.4] K.V. Sriram, M.P. Kothiyal, R.S. Sirohi, "Curvature and focal length measurements using compensation of a collimated beam", *Opt. Laser Technol.*, **23**, 241 (1991).
- [3.5] K. V. Sriram, M. P. Kothiyal, and R. S. Sirohi, "Talbot interferometry in non-collimated illumination for curvature and focal length measurements", *Appl. Opt.*, **31**, 75 (1992).
- [3.6] R. P. Shukla, D. Malacara, "Some applications of the Murty interferometer: A review", *Opt. Lasers. Engg.*, **26**, 1 (1997).
- [3.7] J.S. Darlin, M.P. Kothiyal , R.S. Sirohi, "Wedge plate interferometry: a new dual field configuration for collimation testing", *Opt. Laser Technol.* **30**, 225 (1998).
- [3.8] A. Darudi, M. T. Tavassoly, "Interferometric speci"cation of lens (single and doublet) parameters", *Opt. Lasers Engg.*, **35**, 79 (2001).
- [3.9] V. K. Chhaniwal, A. Anand, and C. S. Narayanamurthy, "Determination of refractive indices of biconvex lenses by use of Michelson interferometer," *Appl. Opt.* **45**, 3985 (2006).
- [3.10] Y. P. Kumar, S. Chatterjee, "Technique for the focal-length measurement of positive lenses using Fizeau interferometry", *Appl. Opt.* **48**, 730 (2009).
- [3.11] S. Reichelt, H. Zappe, "Combined Twyman–Green and Mach–Zehnder interferometer for microlens testing", *Appl. Opt.*, **44**, 5786-5792 (2009).
- [3.12] E. A. Barbosa, C. B. F. de Sousa, W. M. Maffei, "Measurement of low-derivative surface lenses by two-laser holography with $\text{Bi}_{12}\text{TiO}_{20}$ crystals", *Appl. Opt.* **48**, 5114 (2009).
- [3.13] E. A. Barbosa , S. C. dos Santos, "Refractive and geometric lens characterization through multi-wavelength digital speckle pattern interferometry", *Opt. Commun.*, **281**, 1022 (2008).

- [3.14] A. Anand, V. K. Chhaniwal, "Measurement of parameters of simple lenses using digital holographic interferometry and a synthetic reference wave", *Appl. Opt.*, **46**, 2022 (2006).
- [3.15] V. K. Chhaniwal, A. Anand, "Determination of lens parameters with digital holography", *Proc. SPIE*, **6616**, 66164H (2007).
- [3.16] S. Prakash, S. Singh, S. Rana, "Setting sensitivity in collimation testing using Lau interferometry", *J. Opt. A: Pure Appl. Opt.* **8**, 290 (2006).
- [3.17] S. Prakash, S. Rana, S. Prakash, O. Sasaki, "Automated collimation testing using a temporal phase shifting technique in Talbot interferometry", *Appl. Opt.* **5938** (2008).
- [3.18] U. Schnars and W. P. Jueptner, "Digital recording and numerical reconstruction of holograms," *Meas. Sci. Technol.* **13**, R85 (2002).
- [3.19] U. Schnars and W. P. Jueptner, *Digital Holography: Digital Recording, Numerical Reconstruction and Related Techniques* (Springer-Verlag, 2005).
- [3.20] L. Z. Cai, Q. Liu, X. L. Yang, and Y. R. Wang, "Sensitivity adjustable contouring by digital holography and virtual reference wavefront," *Opt. Commun.* **221**, 49 (2003).
- [3.21] "The practical application of light," in *Melles Griot Catalogue for Optical Components* (2000), <http://www.mellesgriot.com>.